# Dual harmonic Kelvin probe force microscopy at the graphene–liquid interface

Liam Collins, Jason I. Kilpatrick, Ivan V. Vlassiouk, Alexander Tselev, Stefan A. L. Weber, Stephen Jesse, Sergei V. Kalinin, and Brian J. Rodriguez

Citation: Applied Physics Letters **104**, 133103 (2014); doi: 10.1063/1.4870074
View online: http://dx.doi.org/10.1063/1.4870074
View Table of Contents: http://scitation.aip.org/content/aip/journal/apl/104/13?ver=pdfcov
Published by the AIP Publishing

# Dual harmonic Kelvin probe force microscopy at the graphene–liquid interface

Liam Collins,[1,2] Jason I. Kilpatrick,[2] Ivan V. Vlassiouk,[3] Alexander Tselev,[4] Stefan A. L. Weber,[2] Stephen Jesse,[4] Sergei V. Kalinin,[4] and Brian J. Rodriguez[1,2,a)]
[1]*School of Physics, University College Dublin, Belfield, Dublin 4, Ireland*
[2]*Conway Institute of Biomolecular and Biomedical Research, University College Dublin, Belfield, Dublin 4, Ireland*
[3]*Energy & Transportation Science Division, Oak Ridge National Laboratory, Oak Ridge, Tennessee 37831, USA*
[4]*Center for Nanophase Materials Sciences, Oak Ridge National Laboratory, Oak Ridge, Tennessee 37831, USA*

(Received 7 February 2014; accepted 20 March 2014; published online 1 April 2014)

Kelvin probe force microscopy (KPFM) is a powerful technique for the determination of the contact potential difference (CPD) between an atomic force microscope tip and a sample under ambient and vacuum conditions. However, for many energy storage and conversion systems, including graphene-based electrochemical capacitors, understanding electrochemical phenomena at the solid–liquid interface is paramount. Despite the vast potential to provide fundamental insight for energy storage materials at the nanoscale, KPFM has found limited applicability in liquid environments to date. Here, using dual harmonic (DH)-KPFM, we demonstrate CPD imaging of graphene in liquid. We find good agreement with measurements performed in air, highlighting the potential of DH-KPFM to probe electrochemistry at the graphene–liquid interface. © *2014 AIP Publishing LLC*. [http://dx.doi.org/10.1063/1.4870074]

Electrochemical phenomena at the solid–liquid interface govern the operation of energy conversion and storage devices, including graphene-based electrochemical capacitors.[1–3] The optimization of such devices requires an understanding of local electrostatics and electrochemistry on the length scale of a single graphene layer, edge, defect, etc.[4,5] In ambient and vacuum environments, the electrochemical or contact potential difference (CPD) between an atomic force microscope (AFM) tip and a sample can be obtained using Kelvin probe force microscopy (KPFM).[6–8] However, there are few tools with nanometer resolution capable of measuring CPD in liquid environments. In KPFM operation, a feedback loop is used to minimize the first harmonic of the electrostatic force through the application of a DC bias, which is proportional to the CPD between the AFM tip and sample. In liquid, the application of DC bias will induce electrochemical processes (e.g., diffuse charge dynamics, electrolysis, Faradaic processes).[9–11] This has led to the development of two approaches which aim to circumvent unwanted electrochemical effects. The first approach is to operate KPFM in non-polar liquids,[12] where the absence of mobile ions effectively suppresses electrochemical processes. The second is to utilize open loop KPFM modes, which do not require bias feedback,[13–17] obviating the requirement for the application of a DC bias.

Previously, we compared open and closed loop operation of KPFM for the measurement of CPD of graphene in air, highlighting the suitability of open loop approaches for eliminating feedback-related offsets in CPD determination.[17] While surface potential values have been reported using open loop KPFM methods implemented in liquid enviroments,[15,16] the true quantitative nature of the approach has yet to be fully realized. Here, to demonstrate the possibility of quantitative open loop KPFM in liquid environments, we use dual harmonic (DH)-KPFM[13–17] to measure and compare CPD values recorded on a model system in both air and milliQ water. To allow a meaningful comparison between air and liquid measurements, and to determine the influence of the imaging environment on CPD measurements, we study graphene, a material known to have stable electrochemical behavior over a large bias range when immersed in liquid.[18] It is widely accepted that electrochemical processes inhibit quantitative CPD measurements, limiting the application of open loop KPFM to date to high frequency and low molarity measurement conditions.[15,16] Here, using the theory of diffuse ion dynamics, we describe why KPFM approaches,[12,15,16] and voltage-modulated scanning probe microscopy in general,[19–21] breakdown in liquids containing mobile ions.

In KPFM, the electrostatic force, $F_{el} = -1/2 C'_z (V_{tip} - V_{cpd})^2$, acting on an AFM probe due to the application of a tip voltage, $V_{tip} = V_{dc} + V_{ac} \sin(\omega t)$, is detected via the first harmonic electrostatic force response of the probe, $F_\omega = -C'_z(V_{dc} - V_{cpd})V_{ac} \sin(\omega t)$, where $V_{dc}$ is a DC bias, $V_{ac}$ is an AC voltage, and $C'_z$ and $V_{cpd}$ are the probe-sample capacitance gradient and CPD, respectively.[6] The second harmonic component of the electrostatic force, $F_{2\omega} = 1/4\, C'_z V_{ac}^2 \cos(2\omega t)$, is independent of CPD and $V_{dc}$ and has proven useful in mapping dielectric properties of samples in both air[22] and low molarity solutions.[23] Whereas the CPD is determined by the $V_{dc}$ which minimizes $F_\omega$ in KPFM, the CPD is determined as $V_{cpd} = sgn(\cos\theta_\omega)(A_\omega/A_{2\omega})(V_{ac}/4X_{gain})$ in DH-KPFM, where $A_\omega$ and $A_{2\omega}$ are the amplitude response of the first and second harmonic electrostatic force, respectively, $X_{gain} = G_\omega/G_{2\omega}$, where $G_\omega$ and $G_{2\omega}$ are the gains due

a)Author to whom correspondence should be addressed. Electronic mail: brian.rodriguez@ucd.ie.

 

to the cantilever transfer function at $\omega$ and $2\omega$, respectively, and $\theta_\omega$ is the phase of the first harmonic response.[12–16]

DH-KPFM measurements were performed in lift mode using an AFM (Asylum Research, MFP-3D), a lock in amplifier (Zurich Instruments, HF2LI), and as-received Pt/Ir-coated (Nanosensors, PPP-EFM) AFM probes with a nominal mechanical resonance frequency and spring constant of 75 kHz and 2.8 N/m, respectively. To prepare the sample investigated in this study, graphene was deposited by chemical vapor deposition on Cu foil (Alfa Aesar, #13382).[24,25]

DH-KPFM was first performed under ambient conditions. For imaging in air, an electrical excitation frequency of 12.5 kHz (well below half the mechanical resonance frequency of the cantilever) with an amplitude of 2 V was used. Figs. 1(a) and 1(b) show the first harmonic mixed ($A_\omega(\cos\theta_\omega)$) and second harmonic amplitude ($A_{2\omega}$) response, respectively, recorded in air. The first harmonic mixed response (Fig. 1(a)) contains information derived from both the magnitude and sign of the charge on the surface with respect to the tip, demonstrating a clear contrast in charge density between Cu and graphene. The second harmonic amplitude (Fig. 1(b)) shows contrast consistent with changes in the capacitance gradient ($C'_z$) related to changes in the probe-sample capacitor geometry. The striped features present on the graphene (Fig. 1(b)) are topographical in nature and are attributed to localized buckling between the graphene and the Cu substrate, induced by thermal relaxation stress during cooling following high temperature (1000 °C) deposition.[24] The CPD in air (Fig. 1(c)) was determined to be $157 \pm 9$ mV and $-47 \pm 5$ mV, for the tip-graphene and tip-Cu interactions, respectively, within the $5 \times 5$ $\mu$m regions indicated in Fig. 1. The relative surface potential difference between graphene and Cu in air is therefore $204 \pm 10$ mV.

Subsequently, DH-KPFM was performed at the same location in milliQ water (Millipore, Gradient A10, 18.2 MΩ·cm) using an excitation frequency of 17.8 kHz with an amplitude of 500 mV. In general, the first harmonic responses in air (Fig. 1(a)) and milliQ water (Fig. 1(d)) were found to show similar contrast, while the second harmonic amplitude responses were noticeably different. In air (Fig. 1(b)), changes in the second harmonic response are attributed to changes in the topographical features. In contrast, the second harmonic response in milliQ water (Fig. 1(e)) shows a material-dependent response. There are a number of possible explanations for this, including changes in the dielectric properties of the surfaces upon immersion in liquid (i.e., oxide formation), or differences in polarizability[26] of the electric double layer at the graphene–liquid or copper–liquid interface. For milliQ water, we determined the CPD in the same $5 \times 5$ $\mu$m locations to be $149 \pm 14$ mV and $-185 \pm 23$ mV for tip-graphene and tip-Cu, respectively. The CPD for tip-graphene is therefore found to agree within experimental error for measurements in both air and milliQ water, as expected.[18] The relative surface potential between graphene and Cu, however, is $334 \pm 27$ mV. Thus, the measured CPD for tip-Cu in liquid has shifted by ~138 mV from the value recorded under ambient conditions. This result is in agreement with recent studies showing that graphene acts as effective inhibitor of air oxidation[27] and a corrosion-inhibitor coating for Cu, where the corrosion rate was inhibited 7-fold in $Na_2SO_4$ solution compared to bare Cu.[18] Graphene has also been shown to effectively inhibit corrosion of Cu foils in physiological environments *in vitro* and *in vivo*.[28] Although we cannot completely rule out influences from the electric double layer or mobile charge dynamics, given the low ion concentration of milliQ water ($\sim 4 \times 10^{-7}$ M),[29] we expect that the observed shift in CPD between air and liquid measurements for Cu but not graphene can be explained by considering that graphene inhibits corrosion on Cu surface.[18,30] These results highlight the potential of DH-KPFM for the quantitative investigation of the graphene–liquid interface, which may elucidate the role that synthesis processes,[31] layer number,[32] and defects[33] have on the electrochemical behavior of graphene materials and devices.[34–36]

For the data shown in Fig. 1, the mechanical cantilever resonance in air shifted from 62.7 kHz to 26.5 kHz in milliQ water due to an increase in the fluid density and enhanced viscous damping. For this reason, we adjusted the electrical drive

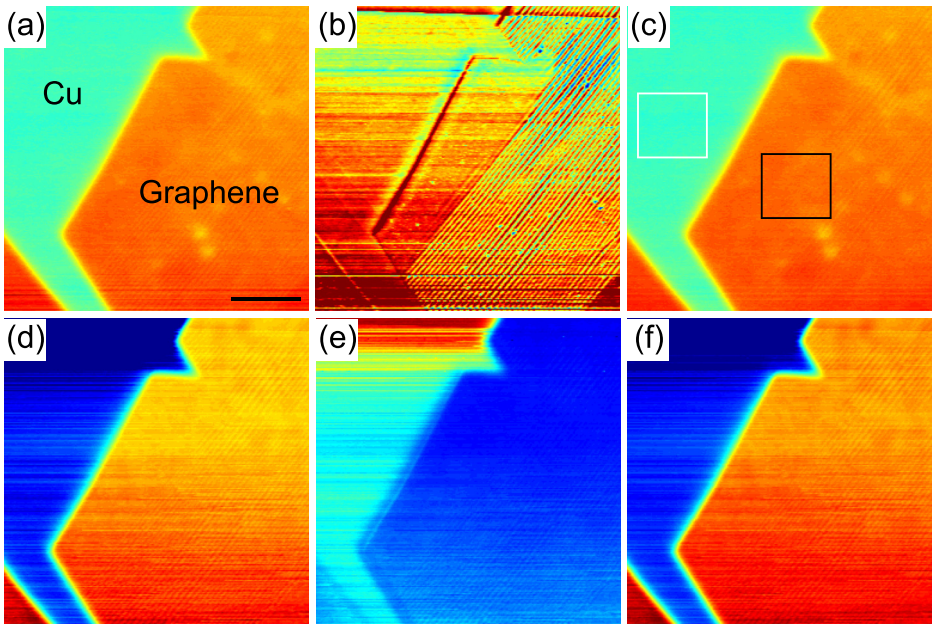


FIG. 1. DH-KPFM images of single layer graphene on Cu foil in (a-c) ambient and (d-f) milliQ water using a lift height of 50 nm (scale bar = 5 $\mu$m). (a and d) First harmonic mixed response images (vertical color scale 5 a.u.) and (b and e) second harmonic amplitude images (vertical color scale 1 a.u.; data offset for clarity). (c and f) CPD (vertical color scale 500 mV).

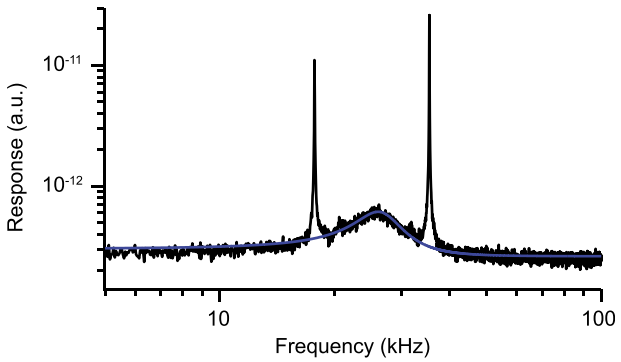


FIG. 2. Thermal noise spectra recorded 50 nm above the graphene surface using the same cantilever as in Fig. 1 with an excitation voltage of 500 mV applied at 17.75 kHz, showing first and second harmonic (35.5 kHz) response located around the mechanical resonance peak (26.5 kHz). A simple harmonic oscillator based fit to the thermal spectra without excitation (blue line) is shown for reference.

frequency to be 2/3 of the mechanical resonance frequency for the data shown in Figs. 1(d)–1(f), thereby positioning the harmonics equidistant from and centered upon the mechanical resonance frequency, as illustrated in Fig. 2. The measurements shown in Fig. 1 were obtained under conditions where the cantilever transfer function was changed markedly by its environment. Therefore, it was imperative to accurately determine $X_{\text{gain}}$ for quantitative measurements. We note also that $X_{\text{gain}}$ depends on tip-sample separation. Thus, $X_{\text{gain}}$ must be determined at the DH-KPFM measurement distance (lift height). The $X_{\text{gain}}$ in milliQ water was determined by fitting a simple harmonic oscillator based model to the thermal noise spectra collected 50 nm above the graphene surface without electrical excitation (blue line in Fig. 2). In air, the $X_{gain}$ was determined during the acquisition of a force curve 50 nm above the surface by measuring the first harmonic response with excitation at $\omega$ and $2\omega$ consecutively to obtain $G_\omega$ and $G_{2\omega}$. Transfer function gains of 0.91 and 0.84 were measured for air and liquid, respectively, and used in the determination of the resultant CPD. Failure to take these $X_{\text{gain}}$ values into account would result in errors of 10% and 19% in the CPD values for air and liquid, respectively. The transfer function gains can also be determined using multifrequency techniques, such as dual amplitude resonance tracking[37] or band excitation.[38] However, the influence of the operating frequency on the measured response depends not only on the cantilever transfer function; it will be further influenced by AC voltage-induced electrochemistry.

DH-KPFM, like all other voltage modulated scanning probe microscopy techniques, is expected to be influenced by the presence of a polar liquid and/or mobile ions, as both the tip- and cantilever-sample interactions will depend strongly on the relaxation processes associated with the motion of the ions and the formation of electric double layers. Thus, for given conditions (e.g., ion concentration), DH-KPFM should be implemented using an excitation frequency such that the electrostatic force is the dominant response mechanism. This may not always be the case, particularly in ion containing solutions where the total force acting on the probe will also have contributions from osmotic pressure (i.e., pressure arising from an ion concentration gradient).[39] For the electrostatic response to dominate, the measurement must be performed on a timescale much shorter than the time it takes for the electric double layers between tip/cantilever-sample to form (i.e., the Debye time), or for ions to diffuse from the bulk to the diffuse electric double layers (i.e., under quasi-static conditions). Following the work of Bazant *et al.*,[40] we have determined that the presence of mobile ions, even in the case of milliQ water, results in a broad distribution of relaxation times (0.23 – 56 ms) in DH-KPFM experiments (Table I). Concentration-dependent time constants (Debye time, $\tau_D$, and charge relaxation, $\tau_C$) occur on a shorter timescale as molarity increases, as shown in Table I. In contrast, the concentration-independent time constant (bulk diffusion, $\tau_L$) is governed by the length scales at which diffusion processes occur, and remains unchanged as the molarity increases.

For milliQ water, the expected Debye screening length ($\lambda$) is on the order of $\sim$ 480 nm.[29] This means that for data shown in Figs. 1 and 2, the tip (separation, L = 50 nm) is well within the expected $\lambda$ and therefore, overlapping electric double layers will have formed. In this case, the tip-sample dynamics is controlled by the Debye time, as tip-sample bulk diffusion processes do not occur. Regarding the data in Fig. 1, it is expected that for an excitation frequency of 17.8 kHz (0.056 ms/cycle), the measurement has been made at timescales shorter than the Debye time and those required for electric double layer charge relaxation and bulk diffusion processes between cantilever-sample electric double layers, resulting in these processes being probed under quasi-static conditions. Also, since our measurement time is faster than the Debye time, milliQ water is expected to behave like a nearly lossless dielectric, as mobile ions do not screen the biased tip. We expect imaging to become unstable in milliQ water when the

TABLE I. Time constants in a DH-KPFM experiment in milliQ water and 100 mM 1:1 electrolyte. The formation of electric double layers is limited by the time it takes an ion to diffuse across the Debye screening length, $\lambda$, and is governed by the Debye time, $\tau_D$.[40] The time constant of ion diffusion from the bulk to the electrodes is $\tau_L$.[40] The charging time of the system can be considered as the charging of two electric double layer capacitances in series with a charge relaxation time of $\tau_C$.[40] The time constants shown are calculated for milliQ water and 100 mM 1:1 electrolyte for the tip-sample ($L = 50$ nm) and cantilever-sample ($L = 15$ $\mu$m) capacitors. The ion diffusivity is set to $D = 1 \times 10^{-9}$ m$^2$/s. In milliQ water for $L = 50$ nm, bulk diffusion is not well-defined due to the overlapping of electric double layers.

| | | | Tip-sample | | Cantilever-sample | |
|---|---|---|---|---|---|---|
| Description | Symbol | Equation | milliQ | 100 mM | milliQ | 100 mM |
| Debye time | $\tau_D$ | $\tau_D = \lambda^2/D$ | 0.23 ms | 0.92 ns | 0.23 ms | 0.92 ns |
| Bulk diffusion | $\tau_L$ | $\tau_L = (L/2)^2/D$ | — | 0.63 $\mu$s | 56 ms | 56 ms |
| Charge relaxation | $\tau_C$ | $\tau_C = \lambda(L/2)/D$ | — | 24 ns | 3.6 ms | 7.2 $\mu$s |

capacitive impedance becomes larger than the solution resistance (i.e., when $f <\sim 1/\tau_D$). At these frequencies, displacement currents at the electrode surface can be smaller than transient currents due to mobile ions in the electrolyte. The results suggest that the agreement observed in CPD measured in air and liquid for graphene stems from both the chemical stability of graphene in milliQ water and operation under quasi-static measurement conditions. For many biological or energy applications, however, operation in high ion concentrations (>100 mM) would be preferred. As the ion concentration increases, electric double layer charge relaxation and Debye times become much faster. For example, in a 100 mM electrolyte, the time taken for an ion to migrate within an applied field (Debye time) is 0.92 ns (Table I). This means that in order to achieve quasi-static equilibrium, an excitation frequency of $>\sim 1.1$ GHz would be required, which is well above the operational frequency of current AFM technology (~MHz). Under such conditions (i.e., in the presence of bias-induced electrochemical phenomena), the dielectric is no longer lossless and the concept of a static CPD becomes invalid, explaining why existing approaches to KPFM breakdown in high molarity (>10 mM) solutions.[12,15,16] Thus, the influence of mobile ions (e.g., charge screening, bulk diffusion, ion crowding) and electrochemical processes on the forces experienced by the probe should to be taken into consideration, necessitating the development of techniques capable of probing the high-frequency bias- and time-dependence of the response.

In this work, we have demonstrated that DH-KPFM can be used to understand local electrostatic and electrochemical phenomena at the solid–liquid interface, which is crucial to areas ranging from corrosion[24,25,41] and sensing[42,43] to biology and biochemistry.[44,45] The results highlight the applicability of DH-KPFM for the investigation of electrochemical processes at the graphene– and other solid–liquid interfaces and potentially near step edges, defects, etc. For operation in high ion concentrations, technical developments are required to circumvent the current instrumental limitations of DH-KPFM imaging.

This publication has emanated from research conducted with the financial support of UCD Research and NANOREMEDIES, which is funded under the Programme for Research in Third Level Institutions Cycle 5 and co-funded by the European Regional Development Fund. This research was supported in part by the Center for Nanophase Materials Sciences, which is sponsored at Oak Ridge National Laboratory by the Scientific User Facilities Division, Office of Basic Energy Sciences, U.S. Department of Energy (CNMS2012-036). The authors are grateful to Zurich Instruments for their support and to N. Balke for insightful discussions. S.A.L.W. acknowledges support from the Alexander von Humboldt Foundation. Some of the measurements were performed on equipment funded by Science Foundation Ireland (SFI07/IN1/B931).

[1]M. Pumera, Energy Environ. Sci. **4**, 668–674 (2010).
[2]T. Y. Kim, H. W. Lee, M. Stoller, D. R. Dreyer, C. W. Bielawski, R. S. Ruoff, and K. S. Suh, ACS Nano **5**, 436–442 (2011).
[3]L. Zhang, F. Zhang, X. Yang, G. Long, Y. Wu, T. Zhang, K. Leng, Y. Huang, Y. Ma, A. Yu, and Y. Chen, Sci. Rep. **3**, 1408 (2013).
[4]S. Banerjee, J. Shim, J. Rivera, X. Jin, D. Estrada, V. Solovyeva, X. You, J. Pak, E. Pop, N. Aluru, and R. Bashir, ACS Nano **7**, 834–843 (2013).
[5]Y. Wenjing, Y. Zhou, Y. Li, C. Li, H. Peng, J. Zhang, Z. Liu, L. Dai, and G. Shi, Sci. Rep. **3**, 2248 (2013).
[6]M. Nonnenmacher, M. P. O'Boyle, and H. K. Wickramasinghe, Appl. Phys. Lett. **58**, 2921–2923 (1991).
[7]A. K. Sinensky and A. M. Belcher, Nat. Nanotechnol. **2**, 653–659 (2007).
[8]F. Mohn, L. Gross, and G. Meyer, Nat. Nanotechnol. **7**, 227–231 (2012).
[9]M. Z. Bazant, M. S. Kilic, B. D. Storey, and A. Ajdari, Adv. Colloid Interface Sci. **152**, 48–88 (2009).
[10]A. C. Hillier, S. Kim, and A. J. Bard, J. Phys. Chem. **100**, 18808–18817 (1996).
[11]R. Raiteri and H. J. Butt, J. Phys. Chem. **99**, 15728–15732 (1995).
[12]A. L. Domanski, E. Sengputa, K. Bley, M. B. Untch, S. A. L. Weber, K. Landfester, C. K. Weiss, H. J. Butt and R. Berger, Langmuir **28**, 13892–13899 (2012).
[13]O. Takeuchi, Y. Ohrai, S. Yoshida, and H. Shigekawa, Jpn. J. Appl. Phys. **46**, 5626 (2007).
[14]L. Collins, J. I. Kilpatrick, M. Bhaskaran, S. Sriram, S. A. L. Weber, S. P. Jarvis, and B. J. Rodriguez, Applications of Ferroelectrics held jointly with 2012 European Conference on the Applications of Polar Dielectrics and 2012 International Symposium on Piezoresponse Force Microscopy and Nanoscale Phenomena in Polar Materials (ISAF/ECAPD/PFM), 2012 International Symposium (IEEE, 2012), pp. 1–4.
[15]N. Kobayashi, H. Asakawa, and T. Fukuma, Rev. Sci. Instrum. **81**, 123705 (2010).
[16]N. Kobayashi, H. Asakawa, and T. Fukuma, J. Appl. Phys. **110**, 044315 (2011).
[17]L. Collins, J. I. Kilpatrick, S. A. L. Weber, A. Tselev, I. V. Vlassiouk, I. N. Ivanov, S. Jesse, S. V. Kalinin, and B. J. Rodriguez, Nanotechnology **24**, 475702 (2013).
[18]D. Prasai, J. C. Tuberquia, R. R. Harl, G. K. Jennings, and K. I. Bolotin, ACS Nano **6**, 1102–1108 (2012).
[19]N. Balke, S. Jesse, Y.-H. Chu, and S. V. Kalinin, ACS Nano **6**, 5559–5565 (2012).
[20]D. J. Marchand, E. Hsiao, and S. H. Kim, Langmuir **29**, 6762–6769 (2013).
[21]B. Kumar and S. R. Crittenden, Nanotechnology **24**, 435701 (2013).
[22]L. Fumagalli, D. E. Ferrer, A. Cuervo, J. L. Carrascosa, and G. Gomilla, Nature Mater. **11**, 808–816 (2012).
[23]G. Gramse, A. Dols-Pérez, M. Edwards, L. Fumagalli, and G. Gomila, Biophys. J. **104**, 1257–1262 (2013).
[24]I. Vlassiouk, M. Regmi, P. Fulvio, S. Dai, P. Datskos, G. Eres, and S. Smirnov, ACS Nano **5**, 6069–6076 (2011).
[25]I. Vlassiouk, P. Fulvio, H. Meyer, N. Lavrik, S. Dai, P. Datskos, and S. Smirnov, Carbon **54**, 58–67 (2013).
[26]O. Cherniavskaya, L. Chen, V. Weng, L. Yuditsky, and L. E. Brus, J. Phys. Chem. B **107**, 1525–1531 (2003).
[27]S. Chen, L. Brown, M. Levendorf, W. Cai, S.-Y. Ju, J. Edgeworth, X. Li, C. W. Magnuson, A. Velamakanni, R. D. Piner, J. Kang, J. Park, and R. S. Ruoff, ACS Nano **5**, 1321–1327 (2011).
[28]W. Zhang, S. Lee, K. L. McNear, T. F. Chung, S. Lee, K. Lee, S. A. Crist, T. L. Ratliff, Z. Zhong, Y. P. Chen, and C. Yang, Sci. Rep. **4**, 4097 (2014).
[29]R. M. Pashley, M. Rzechowicz, L. R. Pashley, and M. J. Francis, J. Phys. Chem. B **109**, 1231–1238 (2005).
[30]L. Nilsson, M. Andersen, R. Balog, E. Lægsgaard, P. Hofmann, F. Besenbacher, B. Hammer, I. Stensgaard, and L. Hornekær, ACS Nano **6**, 10258–10266 (2012).
[31]W. Choi, I. Lahiri, R. Seelaboyina, and Y. S. Kang, Crit. Rev. Solid State **35**, 52–71(2010).
[32]D. W. Wang, F. Li, S. Wu, W. Ren, and H. M. Cheng, Electrochem. Commun. **11**, 1729–1732 (2009).
[33]F. Banhart, J. Kotakoski, and A. V. Krasheninnikov, ACS Nano **5**, 26–41 (2011).
[34]Y. Wang, Z. Shi, Y. Huang, Y. Ma, C. Wang, M. Chen, and Y. Chen, J. Phys. Chem. C **113**, 13103–13107 (2009).
[35]M. D. Stoller, S. Park, Y. Zhu, J. An, and R. S. Ruoff, Nano Lett. **8**, 3498–3502 (2008).
[36]E. J. Yoo, J. Kim, E. Hosono, H. S. Zhou, T. Kudo, and I. Honma, Nano Lett. **8**, 2277–2282 (2008).
[37]B. J. Rodriguez, C. Callahan, S. V. Kalinin, and R. Proksch, Nanotechnology **18**, 475504 (2007).

[38]S. Jesse, S. V. Kalinin, R. Proksch, A. P. Baddorf, and B. J. Rodriguez, Nanotechnology **18**, 435503 (2007).
[39]Y. Yang, K. M. Mayer, and J. Hafner, Biophys. J. **92**, 1966–1974 (2007).
[40]M. Z. Bazant, K. Thornton, and A. Ajdari, Phys. Rev. E **70**, 021506 (2004).
[41]F. Mansfeld, J. Appl. Electrochem. **25**, 187–202 (1995).
[42]T. G. Drummond, M. G. Hill, and J. K. Barton, Nat. Biotechnol. **21**, 1192–1199 (2003).
[43]M. Zhou, Y. Zhai, and S. Dong, Anal. Chem. **81**, 5603–5612 (2009).
[44]H. Hill, Coord. Chem. Rev. **151**, 115–123 (1996).
[45]C. Shan, H. Song, J. Song, D. Han, A. Ivaska, and L. Niu, Anal. Chem. **81**, 2378–2382 (2009).